CHEMICAL PHYSICS

Synergistically enhance confined diffusion by continuum intersecting channels in zeolites

Zhiqiang Liu[1], Jiamin Yuan[1,2], Jasper M. van Baten[3], Jian Zhou[4], Xiaomin Tang[1,2], Chao Zhao[5], Wei Chen[1], Xianfeng Yi[1], Rajamani Krishna[3], German Sastre[6], Anmin Zheng[1]*

In separation and catalysis applications, adsorption and diffusion are normally considered mutually exclusive. That is, rapid diffusion is generally accompanied by weak adsorption and vice versa. In this work, we analyze the anomalous loading-dependent mechanism of *p*-xylene diffusion in a newly developed zeolite called SCM-15. The obtained results demonstrate that the unique system of "continuum intersecting channels" (i.e., channels made of fused cavities) plays a key role in the diffusion process for the molecule-selective pathways. At low pressure, the presence of strong adsorption sites and intersections that provide space for molecule rotation facilitates the diffusion of *p*-xylene along the *Z* direction. Upon increasing the molecular uptake, the adsorbates move faster along the *X* direction because of the effect of continuum intersections in reducing the diffusion barriers and thus maintaining the large diffusion coefficient of the diffusing compound. This mechanism synergistically improves the diffusion in zeolites with continuum intersecting channels.

INTRODUCTION

Diffusion is a common physical phenomenon that affects mass, heat, or momentum and that occurs at both microscopic and macroscopic scales (*1*). In condensed state materials, diffusion may occur in the bulk phase or inside the confined space. The bulk phase diffusion of molecules (or atoms) is often stochastic and is generally referred to as "Brownian movement" (*2*–*4*). However, diffusion inside the confined space is quite different (*5*–*12*).

"Single-file diffusion" is one type of diffusion movement observed inside the confined space (*13*), and it takes place in one-dimensional (1D) channels where the molecules cannot pass each other. Previously, single-file diffusion had been detected in the 1D channels of zeolites using nuclear magnetic resonance (NMR) analysis (*14*–*16*). Molecular dynamics (MD) is another technique that had been used by Sastre and Corma to study the single-file diffusion of benzene and *n*-butane in ITQ-4 and L zeolites. The obtained results demonstrate that in ITQ-4 1D channels, the molecules cannot pass each other, and so, diffusion is single file. However, the wider pores in L zeolite allow for the passage of more than one molecule at a time, resulting in normal diffusion (*17*). In general, single-file diffusion is implicated in 1D channel catalysis and the hydrocarbon traps used in automobiles (*1*, *6*, *18*, *19*). Besides single-file diffusion, "incommensurate diffusion" (*20*, *21*), "levitation effects" (*22*, *23*), "molecular traffic" (*24*), and "inverse shape selectivity" (*25*) have also been observed inside the confined space; however, the mechanisms underlying these effects remain unclear.

The transport of adsorbates in confined channels is controlled by the interplay between adsorbent-adsorbate and adsorbate-adsorbate interactions, as so, molecular diffusion through pores via different mechanisms (*6*, *26*–*34*). Normally, adsorption and diffusion, two primary aspects of practical multidisciplinary applications such as gas separation and heterogeneous catalysis, are considered to be mutually exclusive (i.e., rapid diffusion is generally accompanied by weak adsorption and vice versa). Here, we show that the recently synthesized 3D zeolite SCM-15 (12 × 12 × 10 ring size) (*35*) exhibits unique diffusional behavior compared to other channel-type zeolites (*36*, *37*), with a nonmutually exclusive relationship between adsorption and diffusivity. On the basis of the energy profile and the distribution of adsorption configuration, the role of continuum intersections (i.e., channels made of fused cavities) is established, and the correlation between the unique framework and diffusion behavior is analyzed. The obtained results provide insights into the mechanism of diffusion processes occurring inside confined systems.

RESULTS

Diffusion behavior

The diffusion behavior of molecules inside confined channels is strongly affected by the zeolite framework. As shown in Fig. 1 and fig. S1, the 3D channels of SCM-15 include 12-ring channels along the *X* (6.1 × 6.9 Å), *Y* (5.6 × 6.7 Å), and *Z* (5.9 × 6.3 Å) directions, as well as 10-ring channels along the *Y* (5.1 × 5.5 Å) direction. Notably, two intersections appear in the *XY* and *XZ* planes, and they form "continuum intersecting channels" (i.e., channels made of fused cavities; Fig. 1B) along *X*. The *XY* intersection contains 10- and 12-ring channels along *Y*, both of which cross the 12-ring channels along *X*, resulting in a 12/(10 + 12) ring intersection [6.1 × 6.9/(5.1 × 5.5 + 5.6 × 6.7 Å)] (fig. S2). Meanwhile, the *XZ* intersections are attributed to 12-ring/12-ring channels (6.1 × 6.9/5.9 × 6.3 Å). Unlike the *X* channels, the *Y* and *Z* channels do not intersect, and so, the intersections along *Y* and *Z* axes are discrete (Fig. 1, C and D).

To analyze the movement of guest molecules inside confined channels, the self-diffusion coefficient (D_s) was calculated (*36*, *37*)

[1]State Key Laboratory of Magnetic Resonance and Atomic and Molecular Physics, National Center for Magnetic Resonance in Wuhan, and Key Laboratory of Magnetic Resonance in Biological Systems, Wuhan Institute of Physics and Mathematics, Innovation Academy for Precision Measurement Science and Technology, Chinese Academy of Sciences, Wuhan 430071, P. R. China. [2]University of Chinese Academy of Sciences, Beijing 100049, P. R. China. [3]Van't Hoff Institute for Molecular Sciences, University of Amsterdam, Science Park 904, 1098 XH Amsterdam, Netherlands. [4]Shanghai Research Institute of Petrochemical Technology, SINOPEC, Shanghai 201208, P. R. China. [5]School of Materials Science and Engineering, Zhengzhou University, Zhengzhou, Henan 450001, P. R. China. [6]Instituto de Tecnologia Quimica UPV-CSIC, Universitat Politecnica de Valencia, Av. Los Naranjos s/n, 46022 Valencia, Spain.
*Corresponding author. Email: zhenganm@wipm.ac.cn

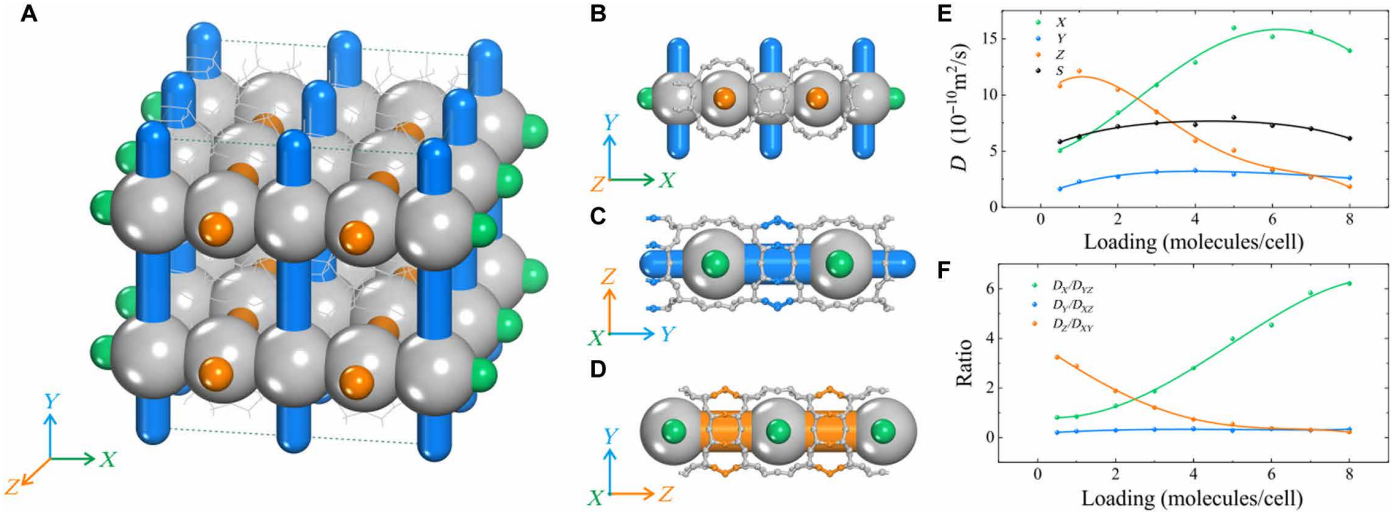

Fig. 1. Channels and diffusion coefficients in the SCM-15 zeolite. (**A**) 3D channels in the SCM-15 zeolite. 1D channels along the (**B**) *X*, (**C**) *Y*, and (**D**) *Z* directions. The silver balls represent intersections. The green, blue, and orange cylinders represent channels along the *X*, *Y*, and *Z* directions, respectively. The small blue and orange balls represent atoms in the *Y* and *Z* channels, respectively (discrete intersections). All atoms in the *X* channels are located in the intersections (continuum intersections), and so, no small green balls are shown. (**E**) Variations in the anisotropic diffusivity of *p*-xylene molecules inside the SCM-15 zeolite as a function of loading (pressure) along the *X*, *Y*, and *Z* directions and as a function of total loading (*S*) at 298 K. (**F**) Variations in anisotropic diffusion coefficient ratio of *p*-xylene molecules as a function of loading (298 K).

using MD. Figure 1E depicts the variation in D_s values of *p*-xylene inside the SCM-15 zeolite as a function of loading (298 K). As shown in the figure, all values are in the order of 10^{-10} m^2/s, which is larger than the D_s values calculated for *p*-xylene molecules in silicate-1 (3D 10-ring channel zeolite, pore size ≈ 5.5 Å, D_s in the order of 10^{-12} m^2/s) (*38*). The difference in self-diffusion coefficient is attributed to the larger pore size of SCM-15 compared to silicate-1. D_s increases at low loading (up to five molecules per cell), and then, it decreases. This behavior is different from that observed in other channel-type zeolites, such as MTW, LTL, AFI, BOG, and MFI, where the diffusion coefficient monotonically decreases with increasing loading (*36*, *37*).

The favorable pathway of *p*-xylene diffusion varies depending on loading. Figure 1F shows that at low loading (0.5 molecules per cell), diffusion in the *Z* direction is about three times faster than that in the *XY* plane (D_Z/D_{XY} ca. 3). However, at high loading (eight molecules per cell), D_Z/D_{XY} markedly changes to 1/5 and D_X/D_{YZ} reaches the high value of ca. 6. Besides *p*-xylene, other molecules such as methane, *n*-butane, and *n*-octane exhibit similar anomalous diffusion behavior inside the SCM-15 zeolite, albeit at varying degrees (fig. S3). Overall, the results show that the preferential pathways of certain molecules inside a zeolite with 3D intersecting channels depend on loading (fig. S4).

Free energy

To understand the effect of loading (pressure) on diffusion behavior, the free energy profile of the diffusing molecule must be analyzed (*25*, *39*). Considering that the diffusion coefficient of *p*-xylene varies only slightly with loading along *Y* (Fig. 1E), the free energy profile corresponding to this direction is not discussed. In the *X* direction, the free energy profile shows two local minima, one in the 12/(10 + 12) ring intersection (q^A, q^E) and the other in the 12-ring/12-ring intersection (q^C) (Fig. 2A), which contribute to ΔE_1 and ΔE_2 energy barriers, respectively. Similarly, the free energy profile along the *Z* direction comprises two energy barriers, $\Delta E_1'$ and $\Delta E_2'$, corresponding to diffusion in the 12-ring straight channels and the 12-ring/12-ring intersection, respectively (Fig. 2B). Figure 2 (C and D) depicts the profiles of ΔE_1, ΔE_2, $\Delta E_1'$, and $\Delta E_2'$ variation as a function of loading. In the channels along the *X* direction, where more molecules are adsorbed in the 12-ring/12-ring and 12/(10 + 12) ring intersections, ΔE_1 and ΔE_2 initially decrease with increasing loading, resulting in an increased diffusion coefficient of *p*-xylene. At high loading (more than five molecules per cell), *p*-xylene diffusion slows down a bit because of the increase in ΔE_2 (Fig. 2C). In the *Z* direction, $\Delta E_1'$ is practically independent of loading; however, $\Delta E_2'$ increases continuously with increasing loading, resulting in slower *p*-xylene diffusion.

Interaction energy

The free energy profiles discussed above provide an understanding of the mechanism underlying loading-dependent *p*-xylene diffusion in different directions. However, they do not explain why diffusion along *Z* is favored at low loading, while at high loading, *p*-xylene diffuses more favorably along *X* (Fig. 1E). The tentative explanation that we propose is that at low loading, the smaller channels along *Z* (5.9 × 6.3 Å) provide a better fit for molecules, whereas at high loading, the larger channels along *X* (6.1 × 6.9 Å) provide more space.

In addition to the free energy profiles, the interaction energy (preferred adsorption sites and interaction energy barriers) and distribution of channel occupancy are important factors affecting *p*-xylene diffusion in different channels. In general, the interaction energy (or adsorption energy) is strongly correlated with the zeolite framework, and thus, variations in local structure lead to differences in interaction energies. The adsorption energy values of *p*-xylene at different locations in SCM-15 are given in Table 1. These values indicate that *p*-xylene is weakly confined in the *XY* and *XZ* intersections where the adsorption energy is lowest (ca. −50 kJ/mol) [points

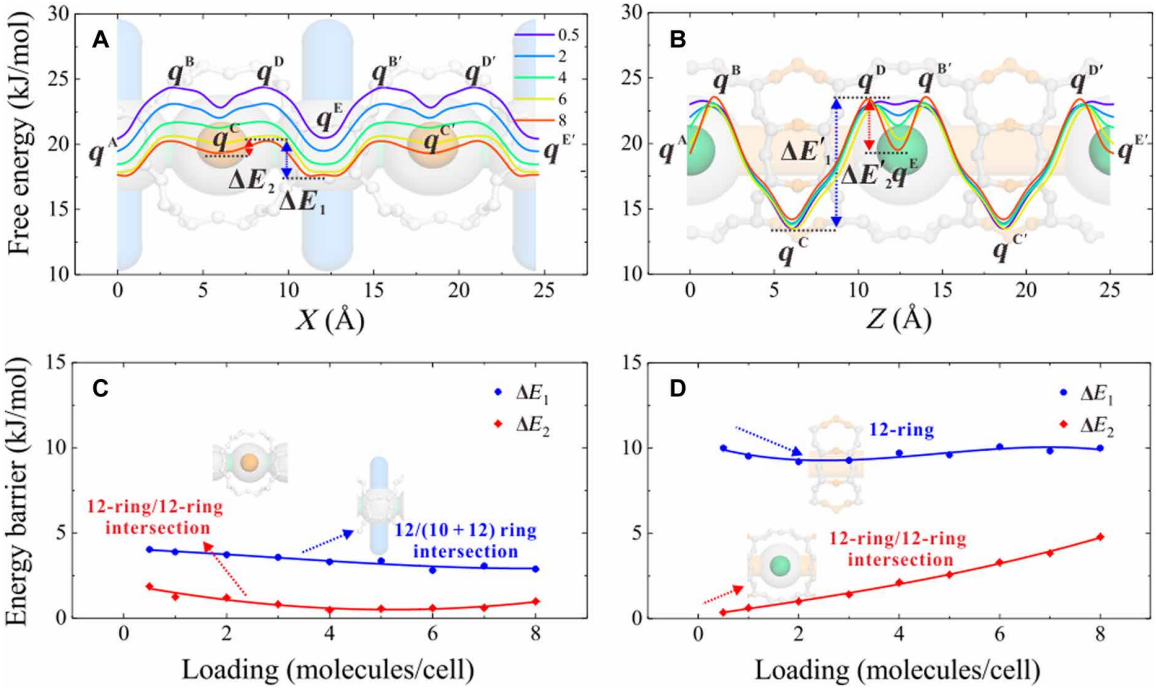

Fig. 2. Free energy profiles and barriers. Free energy profiles of *p*-xylene diffusion along the (**A**) *X* (points A and E located at the 12/(10 + 12) ring intersection and point C located at the 12-ring/12-ring intersection) and (**B**) *Z* (points A and E located at the 12-ring/12-ring intersection and point C located in the 12-ring channel) directions. Variations in the free energy barriers as a function of loading along the (**C**) *X* and (**D**) *Z* directions.

Table 1. Adsorption energy. Adsorption energy of *p*-xylene at selected locations in SCM-15 (locations are shown in Fig. 3).

Point in graph		Location	Energy (kJ/mol)
Fig. 3 (A and D)	A (C and E)	12/(10 + 12) intersection	−51.1
	B (D)	12/12 intersection	−50.3
Fig. 3 (B and E)	A (E)	12-ring	−60.3
	B (D)	12/(10 + 12) intersection	−52.8
	C	10-ring	−73.5
Fig. 3 (C and F)	A (C and E)	12/12 intersection	−52.8
	B (D)	12-ring	−67.5

A and B in Fig. 3 (A and D) and fig. S1A]. In the 12-ring channel segments (not intersection), the adsorption strength is intermediate, with values of ca. −60 kJ/mol along the *Y* direction [5.6 × 6.7 Å; point A in Fig. 3 (B and E) and fig. S1B] and ca. −65 kJ/mol along the *Z* direction [5.9 × 6.3 Å; point B in Fig. 3 (C and F) and fig. S1C]. Last, strong adsorption (ca. −75 kJ/mol) is detected in the 10-ring channels along *Y* [5.1 × 5.5 Å; point C in Fig. 3 (B and E) and fig. S1B]. Knowing that molecules are more likely to be located at sites where adsorption is strongest, *p*-xylene only shows large occupancy of the *X* channels in SCM-15 (lowest adsorption energy) at high loading for its widest sizes.

As shown in Fig. 2 (B and D), the free energy barriers of diffusion along *Z* increase with increasing loading because of the augmentation of the ΔE_2 component (*40*, *41*). Consequently, the diffusivity of *p*-xylene along this direction (D_Z) decreases (Fig. 1E). Along *X*, both energy barriers (ΔE_1 and ΔE_2; Fig. 2, A and C) slightly decrease at higher loading, resulting in increased diffusivity D_X (Fig. 1E). In addition, the order of increasing interaction energy barriers along the *X* (E_X), *Y* (E_Y), and *Z* (E_Z) directions is ΔE_X (2 kJ/mol) < ΔE_Z (15 kJ/mol) < ΔE_Y (30 kJ/mol). This suggests that *p*-xylene molecules can more easily diffuse along the *X* direction than along the *Y* and *Z* directions because of the presence of continuum intersecting channels.

Distribution of channel occupancy

The diffusion behavior of *p*-xylene is also affected by the distribution (location) of molecules in different channels (Fig. 4). Within the investigated loading range (0.5 to 8 molecules per cell), *p*-xylene adsorption in *Z* channels is consistently more favorable than adsorption in *X* and *Y* channels (Fig. 4, A to C), as evidenced by the occupancy distribution presented in Fig. 4D (66 to 56% occupancy in *Z* channels). Note that the distribution of channel occupancy is governed by adsorption energy and entropic factors. Figure 3 shows that, except for the less accessible 10-ring segments along *Y* (adsorption energy, −75 kJ/mol), the 12 rings along the *Z* direction present the large adsorption energy. The large population of *p*-xylene molecules in *Z* channels can thus be explained by strong adsorption and the high accessibility of these channels. Meanwhile, the channels along the *X* direction exhibit the least occupancy due to weak adsorption (adsorption energy, −50 kJ/mol) in the loading range of 0.5 to 8 molecules per cell.

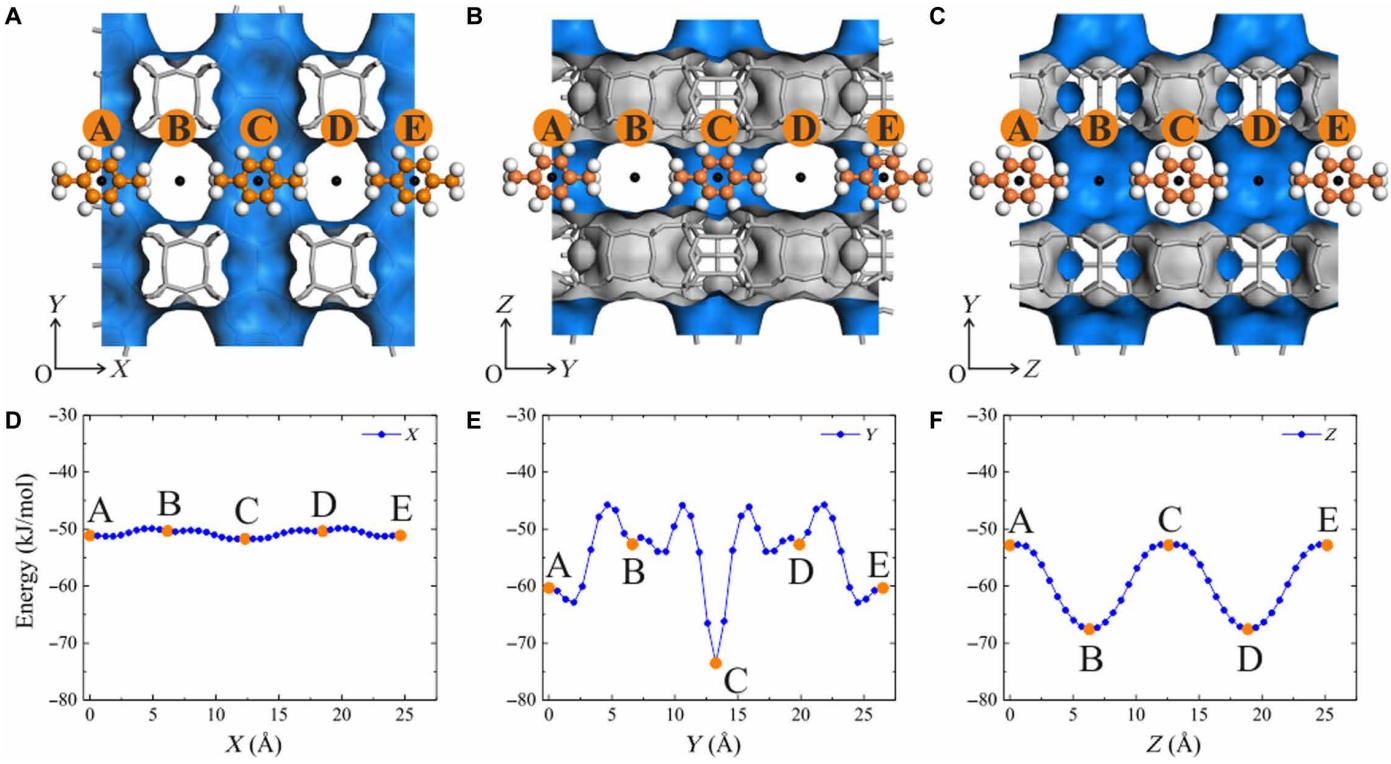

Fig. 3. Diffusion pathways and interaction energy profiles. Definition of *p*-xylene (center of mass) diffusion pathways (points A to E) along the (**A**) *X*, (**B**) *Y*, and (**C**) *Z* directions. The orange, white, and black balls represent C, H, and the center of mass of *p*-xylene, respectively. Interaction energy profiles of *p*-xylene along the (**D**) *X*, (**E**) *Y*, and (**F**) *Z* directions.

Calculations of *p*-xylene molecule orientation in the different channels at different loading (Fig. 5 and fig. S5) further confirm the conclusions drawn above. Considering the large size of intersections, the molecules are preferably oriented in a direction perpendicular to the channel axis, allowing for more effective packing (figs. S6 and S7). This indicates that SCM-15 is a highly tunable zeolite in terms of adsorbate channel distribution at different loadings, which, in turn, affects diffusivity and selectivity. Although temperature (298, 373, and 573 K) does not notable affect channel occupancy (fig. S8), it influences the threshold loading at which diffusivity along the Z direction is overtaken by diffusivity along *X*. The temperature profile of equivalent anisotropic ratio of diffusion coefficients indicates that the threshold loading increases at higher temperatures. At the largest temperature investigated here (573 K), D_z and D_x are similar, irrespective of loading. This shows that when the temperature is high, *p*-xylene molecules will preferably diffuse through the largest channels (*X* and *Z* channels) of SCM-15. Compared to *p*-xylene, other similar molecules such as *o*-xylene and *m*-xylene exhibit different threshold loading, which indicates that selectivity toward *p*-xylene molecules is high (fig. S9).

Figure S3 presents the profiles of methane, *n*-butane, and *n*-octane diffusion in SCM-15 at 298 K. On the basis of these profiles, it may be concluded that larger sorbates are characterized by greater ratios of diffusion coefficients over different channels. In the case of methane, the change in anisotropic diffusion coefficient ratio is small because of the small size of the molecule with respect to the channel. Compared to *p*-xylene, the diffusion behavior of *n*-butane and *n*-octane is quite different, as both compounds preferably diffuse along the *Y* direction at low loading. As loading increases, *n*-octane diffuses primarily along *Z*, with practically no diffusion in the *X* channels that are too long for rotation. Again, the variation in the diffusion behaviors of different compounds allows for greater selectivity of channel occupancy when analyzing mixtures (e.g., *p*-xylene/*n*-octane mixtures).

DISCUSSION

The results reported in this study demonstrate that the SCM-15 porous material characterized by multiple heterogeneous channels along different directions exhibits selective diffusion. The *Z* channels are rich in strong adsorption sites, but they have high diffusion barriers. Meanwhile, the adsorption sites in *X* channels are weak, but diffusion through these barriers requires relatively low energy (low diffusion barrier). The rotation of *p*-xylene molecules in intersections alters the diffusion pathway of these molecules, as shown in Fig. 6. At low loading, diffusion occurs almost exclusively along the *Z* channels comprising many strong adsorption sites (Fig. 6, A and B), while at high loading, diffusion through the *X* channels characterized by low energy barriers (i.e., continuum intersecting channel direction) is favored (Fig. 6, C and D). Such anomalous loading-dependent diffusion behavior can be explained by the particular synergy between adsorption and diffusion.

Furthermore, the diffusion of *p*-xylene molecules in POS and BEC zeolites was also analyzed. These zeolites were chosen because they have continuum intersections similar to those observed in the SCM-15 zeolite (*42*, *43*). The 3D channels in POS are 12-ring

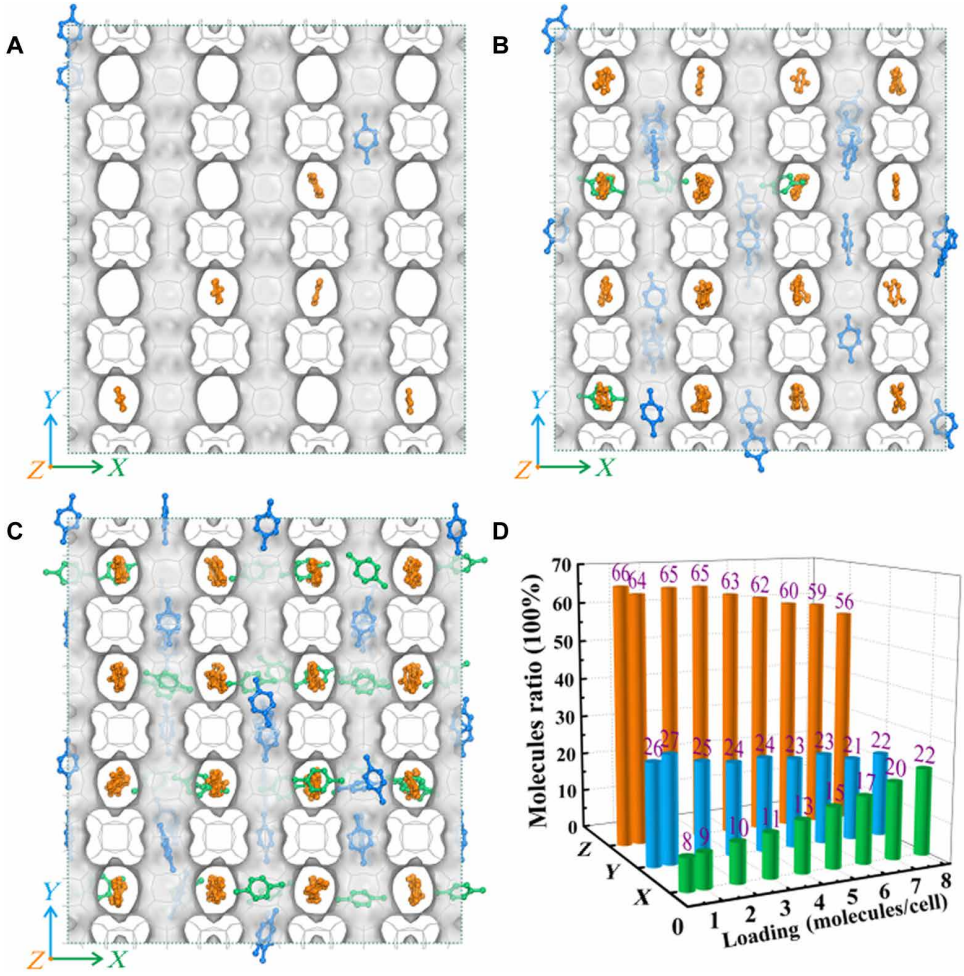

Fig. 4. Channel occupancy in SCM-15 zeolite. Adsorption sites of *p*-xylene inside the SCM-15 zeolite at (**A**) 0.5, (**B**) 4, and (**C**) 8 molecules per cell loading and at 298 K (obtained from MD trajectories; H atoms are omitted for clarity). (**D**) Molecular percentage of *p*-xylene molecules located in *X*, *Y*, and *Z* channels at different loading. Green, blue, and orange colors are used to indicate the locations of *p*-xylene in *X*, *Y*, and *Z* channels, respectively.

channels (7.5 × 6.7 Å) along the *Z* direction and 11-ring channels (4.6 × 6.7 Å) in the *XY* plane. Meanwhile, BEC has 12-ring channels along the *X* (6.0 × 6.9 Å), *Y* (6.0 × 6.9 Å), and *Z* (6.3 × 7.5 Å) directions. Note that two intersections appear in the *XZ* and *YZ* planes of the zeolites and that these intersections form continuum intersecting channels (Fig. 7, A and B). The existence of such channels indicates that similar to the SCM-15 zeolite, the POS and BEC zeolites exhibit pressure-dependent diffusion behavior (Fig. 7, C and D, and fig. S10).

The quick transport of molecules, even small ones such as methane, through microporous channel-type zeolites is considered a great challenge due to the sharp decrease in diffusion coefficients at high loading (fig. S11) (*36*, *37*). Compared to the conventional channel-type zeolites, nanolayer or hierarchical zeolites exhibit improved diffusion; however, their channels cannot be accurately tuned during the synthesis process (*44*, *45*). Therefore, the development of new types of microporous zeolites with excellent diffusion performance is essential. Considering that continuum intersecting channels can substantially reduce the diffusion barrier, regulate molecular rotation, and enhance adsorption at weak adsorption sites, zeolites with such channels (e.g., SCM-15, BEC, and POS zeolites) are highly efficient in separation or catalysis (e.g., xylene and alkanes) applications, especially at high pressure (figs. S7, S9, and S12).

Notably, the anomalous diffusion behavior of hydrocarbons in microporous materials has been reported previously; however, the experimental verification of such behavior constitutes an additional challenge, considering that various effects may be at play, all at once. One of the effects implicated in anomalous diffusion behavior is the "window effect" that describes the unexpected increase in diffusivity of alkanes with growing chain lengths, beyond a certain point (*46*). On the basis of the original work, the diffusivity values reported by Gorring are indirect because these values are extracted from experimental uptake curves without taking into consideration the nonlinearity and thermal effects. A few theoretical models propose alternative means for determining the diffusivity values. For example, Ruthven suggests that the oscillation behavior of apparent diffusivity with carbon number may be accounted for by considering the effects of isotherm nonlinearity and the finite rate of heat dissipation on the adsorption rate. When these effects are taken into account, the unusual profiles of diffusivity or adsorption equilibrium constant variation as a function of carbon number are no longer observed (*47*). Recently, Hwang and coworkers (*48*) have

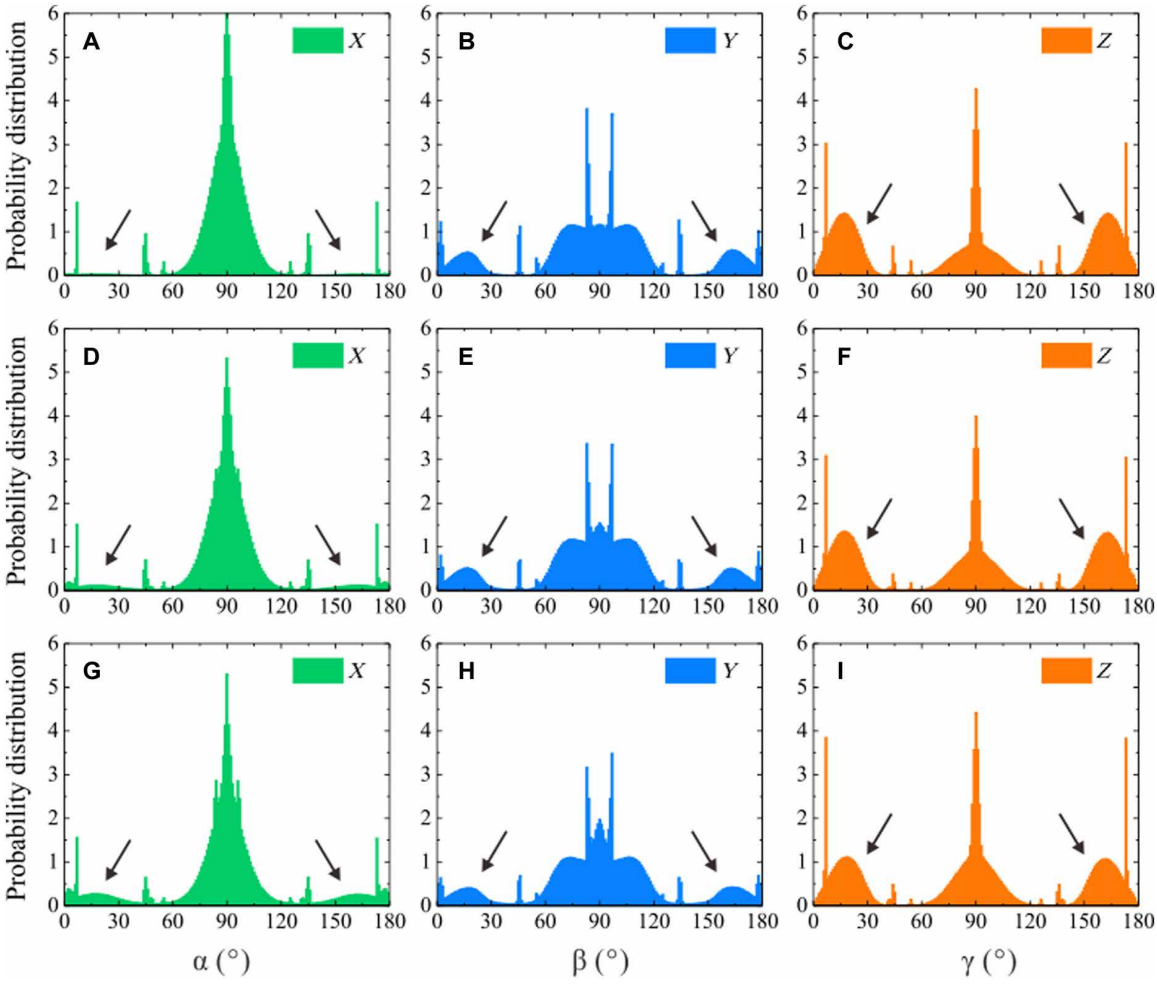

Fig. 5. Molecule orientation in SCM-15 zeolite. Probability distribution of the angle between *p*-xylene molecules and the coordinate axis at the loading of (**A** to **C**) 0.5, (**D** to **F**) 4, and (**G** to **I**) 8 molecules per cell along the *X*, *Y*, and *Z* directions.

experimentally confirmed the anomalous dependence of transport diffusion coefficients on alkane chain length using infrared microimaging and interference. They successfully recorded images of microscopic diffusion under nonequilibrium conditions, with no restrictions regarding the upper limit of the observation time. Using this technique, it was made possible to extend diffusivity measurements to arbitrarily small values. Unlike macroscopic uptake, microimaging measurements are unaffected by the thermal and external transport resistance effects that influence the experimental data in the original interpretation of the window effect. This is mainly due to the fact that in microimaging measurements, diffusion occurs through a bed of crystals. The diffusivities of alkanes comprising two to six carbon atoms in ZIF-4 follow the usual chain-length dependence trend, with *n*-pentane showing maximum diffusivity. The high diffusivity of *n*-pentane may be related to the existence of a window opening wherein configurational shifts facilitate molecular propagation at particular chain lengths.

All the proposed theoretical models agree that the increasing trend in diffusivity at higher alkane chain lengths can only be observed when diffusion occurs in host materials characterized by pore sizes similar to the diameters of the guest molecules. This incommensurate diffusion concept explains why certain long-chain alkanes that are larger than the cage shape exhibit high self-diffusivity, while the smaller hydrocarbons that commensurate with the cage shape remain entrapped and so have low self-diffusivity (*20*, *21*). Although the proposed theoretical models agree considerably well with Gorring's experiments, self-diffusivity (calculated) and transport diffusivity (measured) cannot be directly compared. For instance, the calculated values do not account for the influence of surface effects such as surface barriers (*49*). Other anomalous or rather curious effects such as the levitation effect (*22*, *23*), molecular traffic (*24*), and inverse shape selectivity (*25*) may also influence diffusivity. However, further research is needed to fully comprehend them and to understand how they affect hydrocarbon diffusion in microporous materials. Diffusion in porous media is commonly studied using the well-suited pulsed field gradient (PFG) NMR technique. Notably, this technique has very strict requirements regarding the quality of the sample. For example, PFG NMR requires that the size of the analyzed SCM-15 zeolite crystals be notably larger than 5 μm because self-diffusivity (*D*) in this material is in the order of 10^{-10} m^2/s [according to the Einstein equation: $D = < x >^2/6\Delta$; Δ is the observation time (ca. 40 ms)] (*50*, *51*). So far, large-particle SCM-15 sample with good crystallinity for PFG NMR experiment is a challenge for synthesis, and it is still under progress.

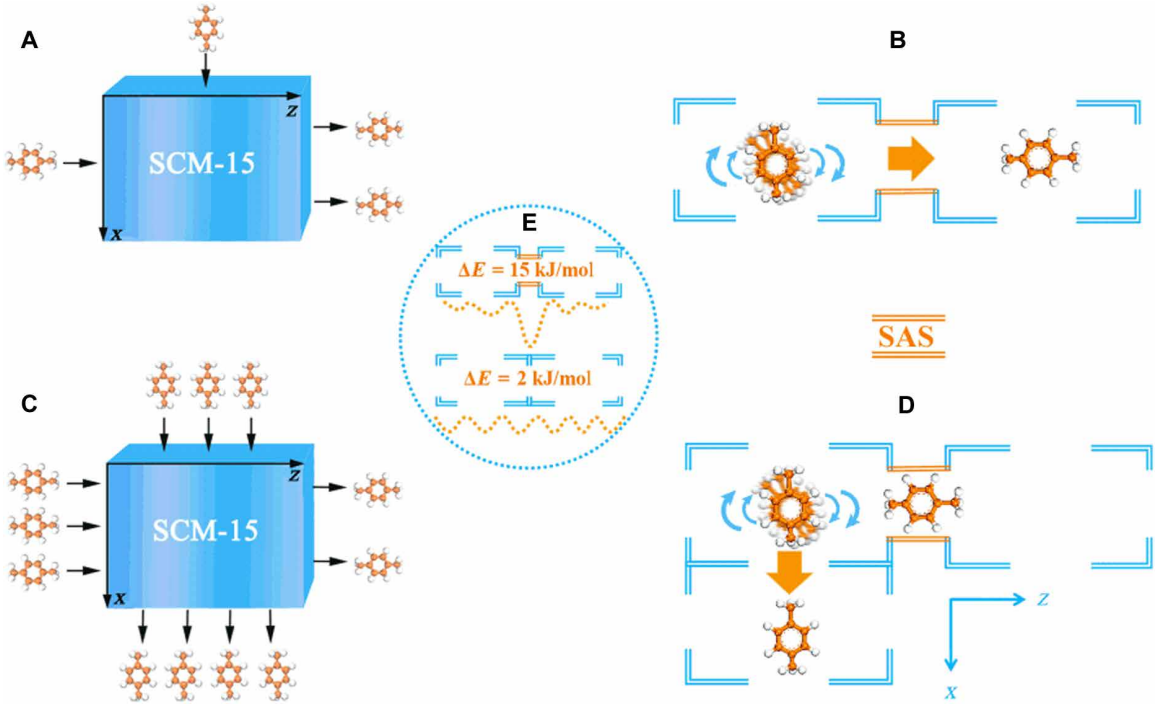

Fig. 6. Mechanism of *p*-xylene diffusion in SCM-15 zeolite. (**A** and **B**) Diffusion mechanism at low loading. The presence of intersections and strong adsorption sites (SAS) along the *Z* direction facilitates the rotation of molecules for self-chosen different directions (movie S1). (**C** and **D**) Diffusion mechanism at high loading. Rotation is efficiently suppressed at high loading because of the preferential occupancy of *p*-xylene along *Z* (movie S2). Therefore, *p*-xylene molecules tend to migrate to the channels along *X*, where they move fast because of the low diffusion barrier at continuum intersections (**E**).

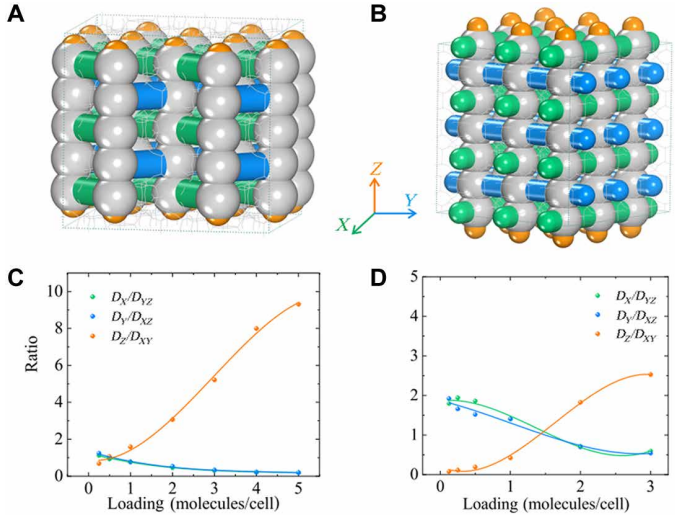

Fig. 7. Channels and diffusion coefficients in POS and BEC zeolites. 3D channels in (**A**) POS and (**B**) BEC zeolites. The silver balls represent intersections. The green, blue, and orange cylinders represent the channels along the *X*, *Y*, and *Z* directions, respectively. Variations in anisotropic diffusion coefficient ratio of *p*-xylene molecules as a function of loading in (**C**) POS and (**D**) BEC zeolites (298 K).

In summary, the 3D intersecting channels in SCM-15 zeolite synergistically enhance the confined diffusion of *p*-xylene. At low loading, the presence of strong adsorption sites and intersections that provide a space for molecule rotation facilitates the diffusion of *p*-xylene molecules along the *Z* direction. Meanwhile, at high loading, *p*-xylene preferentially diffuses along the *X* direction, and it retains its high diffusion coefficient. On the basis of the energy profiles and the adsorbent distribution determined here, the effect of zeolite framework on diffusion has been estimated. The dependence of diffusion behavior on loading has been attributed to the presence of continuum intersecting channels in zeolites with weak adsorption, low diffusion barrier, and large space. This further confirms that continuum intersecting channels promote diffusion at high loading by efficiently reducing the diffusion barriers and by regulating molecular traffic. Consequently, zeolites with continuum intersecting channels (e.g., SCM-15, BEC, and POS) can be tuned for use in the fields of catalysis and separation by controlling the loading and crystal morphology.

METHODS

MD simulation

The initial structure of SCM-15 was taken from the International Zeolite Association database (*52*) and then optimized by GULP (*53*, *54*) using the SLC core-shell force field (*55*, *56*). The supercell dimensions were set at 2 by 2 by 4 unit cell, and *p*-xylene loading was varied between 0.5 and 8 molecules per cell. MD simulations were performed in the canonical ensemble (NVT), where the number of particles (*N*), volume (*V*), and temperature (*T*) are kept constant. The Nosé-Hoover thermostat algorithm was used to control the temperature during simulation and keep it at 298 K (coupling time constant, 0.1 ps). Newton's equations of motion were integrated using the leapfrog Verlet algorithm (time step, 0.5 fs). The

TraPPE-UA (*57*) and TraPPE-zeo (*58*) force fields were used for hydrocarbons and zeolites, respectively (table S1). The Lennard-Jones cross-interaction parameters were determined according to the Lorentz-Berthelot mixing rules, and the cutoff radius was 14 Å. Each MD simulation was equilibrated over 2×10^6 steps, and then, the following 4×10^7 steps were used to study the diffusion behavior of adsorbate molecules. The trajectories were recorded every 1000 steps, and 3 to 15 independent MD simulations were conducted for better statistics. All MD simulations were performed using the DL_POLY 2.0 code (*59*).

Diffusion coefficient

The mean square displacement (MSD) of alkanes is defined by the following equation

$$\mathrm{MSD}(\tau) = \frac{1}{N_m}\sum_{i}^{N_m}\frac{1}{N_\tau}\sum_{t_0}^{N_t}[r_i(t_0+\tau) - r_i(t_0)]^2 \quad (1)$$

where N_m is the number of gas molecules, N_τ is the number of time origins used to calculate the average, and r_i is the coordinate of the ith molecule. The self-diffusion coefficient, D_s, may be determined by calculating the slope of the Einstein relation describing the variation in MSD as a function of time, as shown in Eq. 2

$$\mathrm{MSD}(\tau) = 2nD_s\tau + b \quad (2)$$

where n is the dimension of the zeolite (n = 1 for 1D diffusion, i.e., along the X, Y, or Z directions; n = 2 for 2D diffusion, i.e., along the XY, XZ, or YZ planes; n = 3 for 3D total diffusion). The D_s values reported here were calculated as the average of 3 to 15 independent MD trajectories.

Interaction energy profiles

The interaction energy profiles (*40*, *41*) were determined along the X, Y, and Z directions. To calculate the energy values, a *p*-xylene molecule (center of mass) was first placed in the center of a straight channel; then, it was systematically moved to the center of the adjacent unit cell, following the diffusion path in 40 equidistant steps (Fig. 3). The interaction energy between the framework and *p*-xylene was calculated at each step, and the energy barrier for crossing the channels was determined by calculating the difference between the lowest and highest local energies along the diffusion pathway.

Free energy profile

To explain the diffusion behavior of hydrocarbon molecules passing through the zeolite, the free energy profiles (*60*) were also determined. First, the reaction coordinate of the molecule was chosen along the direction of a unidimensional channel in the zeolite, starting with zero and ending at the extremity of the unit cell (two unit cells in the Z direction). Then, the normalized histogram of the trajectory $\xi(t)$ was established on the basis of the probability distribution $P(\xi)$ of the gas with respect to the direction of channels (ξ represents the coordinate of the center of mass of the molecule). By taking the logarithm of $P(\xi)$, the free energy was obtained, as shown in Eq. 3

$$F(\xi) = -K_\mathrm{B}T\ln P(\xi) \quad (3)$$

where T and K_B are the temperature and Boltzmann's constant, respectively.

SUPPLEMENTARY MATERIALS

Supplementary material for this article is available at http://advances.sciencemag.org/cgi/content/full/7/11/eabf0775/DC1

REFERENCES AND NOTES

1. A. Bunde, J. Caro, J. Kärger, G. Vogl, *Diffusive Spreading in Nature, Technology and Society* (Springer, 2007).
2. P. Langevin, The theory of Brownian movement. *C. R. Hebd. Seances Acad. Sci.* **146**, 530–533 (1908).
3. H. Mori, Transport collective motion and Brownian motion. *Prog. Theor. Phys.* **33**, 423–455 (1965).
4. J. Karger, The random walk of understanding diffusion. *Ind. Eng. Chem. Res.* **41**, 3335–3340 (2002).
5. D. Dubbeldam, E. Beerdsen, S. Calero, B. Smit, Molecular path control in zeolite membranes. *Proc. Natl. Acad. Sci. U.S.A.* **102**, 12317–12320 (2005).
6. B. Smit, T. L. M. Maesen, Molecular simulations of zeolites: Adsorption, diffusion, and shape selectivity. *Chem. Rev.* **108**, 4125–4184 (2008).
7. S. M. Wu, X. Y. Yang, C. Janiak, Confinement effects in zeolite-confined noble metals. *Angew. Chem. Int. Ed.* **58**, 12340–12354 (2019).
8. G.-G. Chang, X.-C. Ma, Y.-X. Zhang, L.-Y. Wang, G. Tian, J.-W. Liu, J. Wu, Z.-Y. Hu, X.-Y. Yang, B. Chen, Construction of hierarchical metal–organic frameworks by competitive coordination strategy for highly efficient CO_2 conversion. *Adv. Mater.* **31**, 1904969 (2019).
9. Y. Chai, X. Han, W. Li, S. Liu, S. Yao, C. Wang, W. Shi, I. Da-Silva, P. Manuel, Y. Cheng, L. D. Daemen, A. J. Ramirez-Cuesta, C. C. Tang, L. Jiang, S. Yang, N. Guan, L. Li, Control of zeolite pore interior for chemoselective alkyne/olefin separations. *Science* **368**, 1002–1006 (2020).
10. A. C. Forse, M. I. Gonzalez, R. L. Siegelman, V. J. Witherspoon, S. Jawahery, R. Mercado, P. J. Milner, J. D. Martell, B. Smit, B. Blumich, J. R. Long, J. A. Reimer, Unexpected diffusion anisotropy of carbon dioxide in the metal-organic framework Zn_2(dobpdc). *J. Am. Chem. Soc.* **140**, 1663–1673 (2018).
11. P. Kortunov, S. Vasenkov, J. Kärger, R. Valiullin, P. Gottschalk, M. F. Elía, M. Perez, M. Stöcker, B. Drescher, G. McElhiney, C. Berger, R. Gläser, J. Weitkamp, The role of mesopores in intracrystalline transport in USY zeolite: PFG NMR diffusion study on various length scales. *J. Am. Chem. Soc.* **127**, 13055–13059 (2005).
12. F. Hibbe, J. Caro, C. Chmelik, A. Huang, T. Kirchner, D. Ruthven, R. Valiullin, J. Karger, Monitoring molecular mass transfer in cation-free nanoporous host crystals of type AlPO-LTA. *J. Am. Chem. Soc.* **134**, 7725–7732 (2012).
13. K. Hahn, J. Karger, V. Kukla, Single-file diffusion observation. *Phys. Rev. Lett.* **76**, 2762–2765 (1996).
14. V. Gupta, S. S. Nivarthi, D. Keffer, A. V. McCormick, H. T. Davis, Evidence of single-file diffusion in zeolites. *Science* **274**, 164–164 (1996).
15. V. Kukla, J. Kornatowski, D. Demuth, I. Gimus, H. Pfeifer, L. V. C. Rees, S. Schunk, K. K. Unger, J. Karger, NMR studies of single-file diffusion in unidimensional channel zeolites. *Science* **272**, 702–704 (1996).
16. Q. Wei, C. Bechinger, P. Leiderer, Single-file diffusion of colloids in one-dimensional channels. *Science* **287**, 625–627 (2000).
17. G. Sastre, A. Corma, Ordinary diffusion and single file diffusion in zeolites with monodimensional channels. Benzene and n-butane in ITQ-4 and L zeolites. *Top. Catal.* **24**, 7–12 (2003).
18. S. Y. Bhide, S. Yashonath, N-pentane and isopentane in one-dimensional channels. *J. Am. Chem. Soc.* **125**, 7425–7434 (2003).
19. K. F. Czaplewski, T. L. Reitz, Y. J. Kim, R. Q. Snurr, One-dimensional zeolites as hydrocarbon traps. *Microporous Mesoporous Mater.* **56**, 55–64 (2002).
20. D. Dubbeldam, S. Calero, T. L. M. Maesen, B. Smit, Incommensurate diffusion in confined systems. *Phys. Rev. Lett.* **90**, 245901 (2003).
21. D. Dubbeldam, B. Smit, Computer simulation of incommensurate diffusion in zeolites: Understanding window effects. *J. Phys. Chem. B* **107**, 12138–12152 (2003).
22. P. K. Ghorai, S. Yashonath, P. Demontis, G. B. Suffritti, Diffusion anomaly as a function of molecular length of linear molecules: Levitation effect. *J. Am. Chem. Soc.* **125**, 7116–7123 (2003).
23. S. Nag, G. Ananthakrishna, P. K. Maiti, S. Yashonath, Separating hydrocarbon mixtures by driving the components in opposite directions: High degree of separation factor and energy efficiency. *Phys. Rev. Lett.* **124**, 255901 (2020).
24. E. G. Derouane, Z. Gabelica, A novel effect of shape selectivity: Molecular traffic control in zeolite ZSM-5. *J. Catal.* **65**, 486–489 (1980).

25. M. Schenk, S. Calero, T. L. M. Maesen, L. L. van Benthem, M. G. Verbeek, B. Smit, Understanding zeolite catalysis: Inverse shape selectivity revised. *Angew. Chem. Int. Ed.* **41**, 2500–2502 (2002).
26. P. Cnudde, R. Demuynck, S. Vandenbrande, M. Waroquier, G. Sastre, V. Speybroeck, Light olefin diffusion during the MTO process on H-SAPO-34: A complex interplay of molecular factors. *J. Am. Chem. Soc.* **142**, 6007–6017 (2020).
27. H. Jobic, A. Methivier, G. Ehlers, B. Farago, W. Haeussler, Accelerated diffusion of long-chain alkanes between nanosized cavities. *Angew. Chem. Int. Ed.* **43**, 364–366 (2004).
28. D. Dubbeldam, S. Calero, T. L. M. Maesen, B. Smit, Understanding the window effect in zeolite catalysis. *Angew. Chem. Int. Ed.* **42**, 3624–3626 (2003).
29. M. Gao, H. Li, W. Liu, Z. Xu, S. Peng, M. Yang, M. Ye, Z. Liu, Imaging spatiotemporal evolution of molecules and active sites in zeolite catalyst during methanol-to-olefins reaction. *Nat. Commun.* **11**, 3461 (2020).
30. M. H. Sun, S. Z. Huang, L. H. Chen, Y. Li, X. Y. Yang, Z. Y. Yuan, B. L. Su, Applications of hierarchically structured porous materials from energy storage and conversion, catalysis, photocatalysis, adsorption, separation, and sensing to biomedicine. *Chem. Soc. Rev.* **45**, 3479–3563 (2016).
31. S. Peng, M. B. Gao, H. Li, M. Yang, M. Ye, Z. Liu, Control of surface barriers in mass transfer to modulate methanol-to-olefins reaction over SAPO-34 zeolites. *Angew. Chem. Int. Ed.* **59**, 21945–21948 (2020).
32. S. E. Jee, D. S. Sholl, Carbon dioxide and methane transport in DDR zeolite: Insights from molecular simulations into carbon dioxide separations in small pore zeolites. *J. Am. Chem. Soc.* **131**, 7896–7904 (2009).
33. Y. Li, J. Yu, New stories of zeolite structures: Their descriptions, determinations, predictions, and evaluations. *Chem. Rev.* **114**, 7268–7316 (2014).
34. J. Zhou, Y. Wang, W. Zou, C. Wang, L. Li, Z. Liu, A. Zheng, D. Kong, W. Yang, Z. Xie, Mass transfer advantage of hierarchical zeolites promotes methanol converting into *para*-methyl group in toluene methylation. *Ind. Eng. Chem. Res.* **56**, 9310–9321 (2017).
35. Y. Luo, S. Smeets, Z. Wang, J. Sun, W. Yang, Synthesis and structure determination of SCM-15: A 3D large pore zeolite with interconnected straight 12×12×10-ring channels. *Chem. A Eur. J.* **25**, 2184–2188 (2019).
36. E. Beerdsen, D. Dubbeldam, B. Smit, Loading dependence of the diffusion coefficient of methane in nanoporous materials. *J. Phys. Chem. B* **110**, 22754–22772 (2006).
37. E. Beerdsen, D. Dubbeldam, B. Smit, Understanding diffusion in nanoporous materials. *Phys. Rev. Lett.* **96**, 044501 (2006).
38. P. D. Kolokathis, G. Kali, H. Jobic, D. N. Theodorou, Diffusion of aromatics in silicalite-1: Experimental and theoretical evidence of entropic barriers. *J. Phys. Chem. C* **120**, 21410–21426 (2016).
39. E. Beerdsen, D. Dubbeldam, B. Smit, Molecular understanding of diffusion in confinement. *Phys. Rev. Lett.* **95**, 164505 (2005).
40. G. Sastre, C. R. A. Catlow, A. Corma, Diffusion of benzene and propylene in MCM-22 zeolite. A molecular dynamics study. *J. Phys. Chem. B* **103**, 5187–5196 (1999).
41. S. Gao, Z. Liu, S. Xu, A. Zheng, P. Wu, B. Li, X. Yuan, Y. Wei, Z. Liu, Cavity-controlled diffusion in 8-membered ring molecular sieve catalysts for shape selective strategy. *J. Catal.* **377**, 51–62 (2019).
42. W. Hua, H. Chen, Z. B. Yu, X. Zou, J. Lin, J. Sun, A germanosilicate structure with 11×11×12-ring channels solved by electron crystallography. *Angew. Chem. Int. Ed.* **53**, 5868–5871 (2014).
43. G. Sastre, J. A. Vidal-Moya, T. Blasco, J. Rius, J. L. Jorda, M. T. Navarro, F. Rey, A. Corma, Preferential location of Ge atoms in polymorph C of beta zeolite (ITQ-17) and their structure-directing effect: A computational, XRD, and NMR spectroscopic study. *Angew. Chem. Int. Ed.* **41**, 4722–4726 (2002).
44. D. Schneider, D. Mehlhorn, P. Zeigermann, J. Karger, R. Valiullin, Transport properties of hierarchical micro-mesoporous materials. *Chem. Soc. Rev.* **45**, 3439–3467 (2016).
45. J. Perez-Ramirez, C. H. Christensen, K. Egeblad, C. H. Christensen, J. C. Groen, Hierarchical zeolites: Enhanced utilisation of microporous crystals in catalysis by advances in materials design. *Chem. Soc. Rev.* **37**, 2530–2542 (2008).
46. R. L. Gorring, Diffusion of normal paraffins in zeolite T Occurrence of window effect. *J. Catal.* **31**, 13–26 (1973).
47. D. M. Ruthven, The window effect in zeolitic diffusion. *Microporous Mesoporous Mater.* **96**, 262–269 (2005).
48. S. Hwang, A. Gopalan, M. Hovestadt, F. Piepenbreier, C. Chmelik, M. Hartmann, R. Q. Snurr, J. Kärger, Anomaly in the chain length dependence of n-alkane diffusion in ZIF-4 metal-organic frameworks. *Molecules* **13**, 668 (2018).
49. G. Sastre, J. Kärger, D. M. Ruthven, Molecular dynamics study of diffusion and surface permeation of benzene in silicalite. *J. Phys. Chem. C* **122**, 7217–7225 (2018).
50. A. Einstein, *Investigations on the Theory of Brownian Movement* (Dover Publications, 1926), p 119.
51. W. Dai, M. Scheibe, L. Li, N. Guan, M. Hunger, Effect of the methanol-to-olefin conversion on the PFG NMR self-diffusivities of ethane and ethene in large-crystalline SAPO-34. *J. Phys. Chem. C* **116**, 2469–2476 (2012).
52. C. Baerlocher, L. B. McCusker, *Database of Zeolite Structures* (2016); www.iza-structure.org/databases/ [accessed June 2016].
53. J. D. Gale, GULP: A computer program for the symmetry-adapted simulation of solids. *J. Chem. Soc. Faraday Trans.* **93**, 629–637 (1997).
54. J. D. Gale, A. L. Rohl, The general utility lattice program (GULP). *Mol. Simulat.* **29**, 291–341 (2003).
55. C. R. A. Catlow, C. M. Freeman, B. Vessal, S. M. Tomlinson, M. Leslie, Molecular dynamics studies of hydrocarbon diffusion in zeolites. *J. Chem. Soc. Faraday Trans.* **87**, 1947–1950 (1991).
56. M. J. Sanders, M. Leslie, C. R. A. Catlow, Interatomic potentials for SiO_2. *J. Chem. Soc. Chem. Comm.* **1984**, 1271–1273 (1984).
57. C. D. Wick, M. G. Martin, J. I. Siepmann, Transferable potentials for phase equilibria. 4. United-atom description of linear and branched alkenes and alkylbenzenes. *J. Phys. Chem. B* **104**, 8008–8016 (2000).
58. P. Bai, M. Tsapatsis, J. I. Siepmann, TraPPE-zeo: Transferable potentials for phase equilibria force field for all-silica zeolites. *J. Phys. Chem. C* **117**, 24375–24387 (2013).
59. W. Smith, T. R. Forester, DL_POLY_2.0: A general-purpose parallel molecular dynamics simulation package. *J. Mol. Graph.* **14**, 136–141 (1996).
60. A. Ghysels, S. L. C. Moors, K. Hemelsoet, K. De Wispelaere, M. Waroquier, G. Sastre, V. Van Speybroeck, Shape-selective diffusion of olefins in 8-ring solid acid microporous zeolites. *J. Phys. Chem. C* **119**, 23721–23734 (2015).

Acknowledgments: We are grateful to the Shenzhen Cloud Computing Center for allowing the use of their computing facilities. **Funding:** This work was supported by the National Natural Science Foundation of China (nos. 22032005, 21902180, 21802164, 21991092, 21991090, 22002174, and 91645112), the Natural Science Foundation of Hubei Province of China (2018CFA009), the Key Research Program of Frontier Sciences (CAS no. QYZDB-SSW-SLH026), Sinopec Corp. (417012-4), and the CAS Interdisciplinary Innovation Team (grant no. JCTD-2018-10). G.S. thanks the MICINN of Spain for funding through projects RTI2018-101784-B-I00, RTI2018-101033-B-I00, and SEV-2016-0683. **Author contributions:** A.Z. formulated the project. Z.L., J.Y., X.T., C.Z., and W.C. performed the MD simulations. Z.L., J.M.v.B., J.Z., X.Y., R.K., G.S., and A.Z. analyzed the data. Z.L., G.S., and A.Z. wrote the manuscript. All the authors read and commented on the manuscript. **Competing interests:** The authors declare that they have no competing interests. **Data and materials availability:** All data needed to evaluate the conclusions in the paper are present in the paper and/or the Supplementary Materials. The primary data that support the plots and other findings reported in this study may be requested from the corresponding author.

Submitted 2 October 2020
Accepted 28 January 2021
Published 12 March 2021
10.1126/sciadv.abf0775

Citation: Z. Liu, J. Yuan, J. M. van Baten, J. Zhou, X. Tang, C. Zhao, W. Chen, X. Yi, R. Krishna, G. Sastre, A. Zheng, Synergistically enhance confined diffusion by continuum intersecting channels in zeolites. *Sci. Adv.* **7**, eabf0775 (2021).